Formation yield of germanium-vacancy centers in diamond upon keV ion nano-implantation and thermal annealing

Journal of Applied Physics

RESEARCH ARTICLE | JULY 22 2025

Formation yield of germanium-vacancy centers in diamond upon keV ion nano-implantation and thermal annealing

Special Collection: Defects in Solids for Quantum Technologies

Vanna Pugliese ; Gaia Gavello ; Elena Nieto Hernandez ; Elisa Redolfi ; Elia Scattolo ; Alessandro Cian ; Elena Missale ; Alberto Bortone ; Rossana Dell'Anna ; Sviatoslav Ditalia Tchernij ; Damiano Giubertoni ; Jacopo Forneris

J. Appl. Phys. 138, 044401 (2025)
https://doi.org/10.1063/5.0258262

Journal of Applied Physics ARTICLE pubs.aip.org/aip/jap

Formation yield of germanium-vacancy centers in diamond upon keV ion nano-implantation and thermal annealing

Cite as: J. Appl. Phys. **138**, 044401 (2025); doi: 10.1063/5.0258262
Submitted: 15 January 2025 · Accepted: 30 June 2025 ·
Published Online: 22 July 2025

Vanna Pugliese,[1,2] Gaia Gavello,[1,3] Elena Nieto Hernandez,[1,2] Elisa Redolfi,[1,2] Elia Scattolo,[4] Alessandro Cian,[4] Elena Missale,[4] Alberto Bortone,[2] Rossana Dell'Anna,[4] Sviatoslav Ditalia Tchernij,[1,2] Damiano Giubertoni,[4,a)] and Jacopo Forneris[1,2]

AFFILIATIONS

[1]Physics Department, Università di Torino, 10125 Torino, Italy
[2]Istituto Nazionale di Fisica Nucleare (INFN), Sezione di Torino, 10125 Torino, Italy
[3]Dipartimento di Scienza e Tecnologia Applicata, Politecnico di Torino, 10129 Torino, Italy
[4]Center for Sensors and Devices (SD), FBK—Fondazione Bruno Kessler, 38123 Trento, Italy

Note: This paper is part of the Special Topic, Defects in Solids for Quantum Technologies.
[a)]**Author to whom correspondence should be addressed:** giuberto@fbk.eu

ABSTRACT

Group-IV-related color centers in diamond are promising systems in the framework of solid-state quantum technologies. A key enabler for the integration of these emitters in real-world devices consists of their reliable fabrication by means of controlled engineering processes such as deterministic ion implantation. In this work, the formation yield of the negatively charged germanium-vacancy (GeV^-) center in diamond upon keV ion implantation and subsequent thermal annealing was investigated. A systematic fabrication approach was adopted, exploiting focused ion beam technology to take advantage of nanometric spatial accuracy and a controllable implantation fluence. The photoluminescence analysis of the implanted spots, including single emitter characterization, enables the direct quantification of the GeV^- center formation yield under the implemented fabrication approach.

I. INTRODUCTION

Diamond represents a competitive platform for quantum technologies due to its suitability to host color centers in its lattice.[1–3] These optically active defects are appealing candidates for the solid-state implementation of stable single-photon sources (SPS), allowing the development of quantum photonics protocols and enabling the implementations of challenging measurements at the nanoscale, potentially including biological samples' properties.[4–7] In addition, they can act as qubits used for quantum computation,[8,9] quantum memories, or quantum repeaters,[10–12] depending on the properties of the specific emitter.

Several types of color centers have been studied so far, each standing with peculiar properties for specific quantum-enhanced applications. The Nitrogen-Vacancy (NV) center is the most studied defect due to the possibility to readout and drive its spin state.[13,14] Group-IV centers[3,15–18] have also emerged as valid alternatives, thanks to their narrow emission spectrum and intense photon count rate, for single-photon applications in which the broad spectral photoluminescence (PL) of the NV center is inconvenient. Moreover, the limited response to environmental stimuli and external field fluctuations, owed to the split-vacancy structural symmetry of group-IV color centers, is a desirable feature for all those applications requiring minimal environmental perturbations.[19,20] In this regard, the GeV^- center can be regarded as an appealing candidate due to the intense PL emission at 602 nm,[21] a high Debye–Waller factor (of ~60%, Refs. 16, 22), and experimentally proven temperature and pressure sensing capabilities.[23–25]

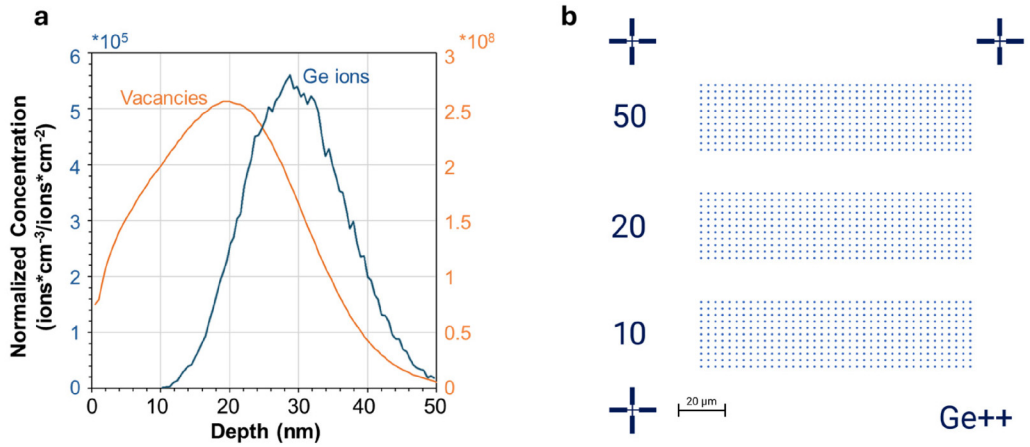

FIG. 1. (a) SRIM simulation of the vacancies distribution in orange and the Ge ions in blue, regarding the implantation of Ge^{++} ions accelerated with a voltage of 35 kV and implanted into a diamond substrate. (b) Example of the adopted design: dose labels and cross fiducial markers were irradiated with Au ions whereas the spot array with Ge ions.

The crucial challenge separating these appealing systems from technological uptake is a reliable fabrication process, which should be ideally deterministic and scalable.[2,3] The most common approach adopted for color centers in diamond relies on ion implantation followed by subsequent thermal annealing.[26,27] Ion implantation indeed enables in principle to deliver an exact number of ions at specific impact locations on the target with sub-100 nm position accuracy.[28–31] This level of precision is within the specifications of focused ion beam (FIB) technology.[32] FIB systems offer precise control over ion dosage, spatial positioning, and beam current, enabling accurate manipulation of ion implantation parameters essential for the reliable formation of color centers. With the recent development of custom ion sources based on eutectic alloys,[33] FIB-based ion implantation offers the capability to address the fabrication of group-IV impurities in diamond.[34,35] The scalability challenge, thus, lies in the formation yield of the desired color center, i.e., the ratio between optically active color centers and implanted impurities in the substrate.[26] An accurate estimation of the formation yield for a specific set of implantation and processing parameters is, thus, crucial to identify pathways toward the maximization of the fabrication efficiency, enabling greater control over color center properties and consistency.

The present work focuses on the quantification of the negatively charged germanium-vacancy (GeV^-) center formation yield in diamond upon keV ion implantation and thermal annealing. We fabricate an array of Ge-implanted spots using a nanoscale focused ion beam (FIB), by varying the predetermined number of impinging ions, i.e., the ion fluence. Following a high-temperature annealing, the analysis of the PL intensity of the implanted spots normalized to the photon emission of individual GeV^- centers enables the direct quantification of the formation yield of the defect under the considered manufacturing conditions.

II. EXPERIMENTAL METHODS

A. Sample fabrication

The fabrication of GeV^- color centers presented in this work was performed by perpendicular ion implantation using the Raith Velion FIB-SEM system installed in the Fondazione Bruno Kessler (FBK) laboratories. It is equipped with a liquid metal alloy ion source (Si-Ge-Au) and with a Wien filter to select the desired ion species. The ion optics allows a focused ion beam spot size down to 15 nm for 35 kV accelerated $^{74}Ge^{++}$ ion beam. The latter in synergy with a laser interferometric sample holder stage enables the delivery of a controllable ion fluence with nanometric spatial resolution. Furthermore, the implantation fluence, although determined by Poisson statistics, can reach the single ion level, thanks to the pA beam current and a minimum programmable dwell time of 20 ns.

The fabrication was performed using the 35 kV accelerated $^{74}Ge^{++}$ (70 keV kinetic energy) ion beam, impinging on a single crystal electronic grade diamond substrate (substitutional N and B concentrations below 5 ppb) to limit the concurrence of other defects related to native lattice impurities.

According to Monte Carlo SRIM (Stopping and Range of Ions in Matter) simulations[36] performed assuming a displacement energy of 50 eV,[37] a diamond density of 3.51 g/cm^3, and neglecting channeling effects, the calculated longitudinal projected range R_p for the Ge ions is ~29 nm [Fig. 1(a)], while the distribution of projectile-induced vacancies in the crystal lattice is peaked at 20 nm depth. Since vacancies are essential to form the luminescent defects, the apparent overlap between the two profiles plotted in Fig. 1(a) is compatible with the formation of GeV^- centers.

A preliminary irradiation with Au^+ ions was carried out to fabricate fiducial markers and labels identifying the regions of interest. The $^{74}Ge^{++}$ implantation was performed by irradiating single spots (corresponding to the only opening of the beam) distributed in arrays of 400 points, 3 μm spaced apart, at nine different

TABLE I. Average PL counts in the 600–650 nm spectral range over 32 emitting spots of each implanted matrix, acquired at a fixed optical power of 0.7 mW. A Poissonian uncertainty is associated with the spot dose values; fluence values are calculated assuming a 15 nm diameter beam spot, while the uncertainty associated with the counts is determined considering the background subtraction and the averaging operations.

Spot dose (ions/spot)	660 ± 30	460 ± 20	330 ± 20	265 ± 16	132 ± 11	66 ± 8
Fluence (ions/cm^2) × 10^{13}	40 ± 20	26 ± 16	18 ± 11	15 ± 9	7 ± 4	4 ± 2
PL counts (kcps)	149 ± 5	123 ± 6	99 ± 7	82 ± 6	36 ± 4	28 ± 4

fluences. In the following, ion fluence (defined as the number of ions implanted per surface unit) will be expressed in terms of ion spot dose, defined as the nominal number of ions implanted at each target point of the array. Implantations were performed with spot doses ranging from 7 to 660 ions per spot. The adopted layout is displayed in Fig. 1(b). The estimation of the beam spot size was carried out by a "knife edge method" according to ISO/TR 19319:2013. A secondary electron image was acquired scanning the ion beam on a sample with gold spherical nanoparticles deposited on a carbon tape, i.e., a sample providing excellent contrast and sharp edges at the nanometric level. Contrast line scans were extrapolated from the image, on both x- and y-axes across the sharp edges of a gold nanoparticle. The beam size was then estimated as the width where the signal raised from 20% to 80% of the contrast excursion, for both x- and y-line scans. The average of the two values and relative uncertainties linked to the contrast curve noise resulted in an estimation of the beam size of (15 ± 5) nm achieved at an ion current of ∼2 pA. Therefore, the ion spot dose range chosen for the implantations corresponds to fluences comprised in the $(0.4–40) \times 10^{13}$ cm^{-2} range, of which only the $(4–40) \times 10^{13}$ cm^{-2} fluence range allowed the detection of GeV$^-$ luminescence, with the outcome included in Table I. Following ion implantation, the sample was thermally annealed at 900 °C for 2 h, to restore the damaged lattice and to favor the formation of GeV$^-$ centers. This process was performed in a furnace based on a ceramic heater, under high vacuum conditions ($<5 \times 10^{-6}$ mbar).

B. Optical characterization

The room-temperature photoluminescence of the fabricated color centers was analyzed by means of a custom confocal microscope. A three-axis piezoelectric positioner was used to scan the sample with nanometric accuracy, enabling high resolution PL imaging by means of a high magnification, high numerical aperture dry objective (100×, 0.9 N.A.). A continuous wave 522 nm laser diode was exploited to properly excite the GeV$^-$ centers. The PL emission was directed through a long-pass dichroic mirror with a cutoff wavelength at 567 nm. Additional optical filters were employed to reject both the laser emission and the diamond Raman line at 561 nm (1332 cm^{-1}). In detail, two filtering combinations were adopted: one with a long-pass filter at 565 nm and another including a long-pass filter at 600 nm together with a 650 nm short-pass filter to solely select the GeV$^-$ spectral contribution. The lateral resolution of the confocal microscope was approximately 400 nm, as determined by the investigated wavelength range and by the employed objective. The collected PL was focused into the core of a fiber-fused 50:50 beam splitter. In this way, two commercial Silicon-based Single Photon Avalanche Diodes (Si-SPAs) were coupled using optical multimode fibers to the microscope in order to measure the PL count rate as well as to assess the single-photon emission of GeV$^-$ centers by means of Hanbury-Brown and Twiss (HBT) interferometry.[38] Alternatively, one of the two output fibers was coupled to a monochromator to spectrally analyze the gathered PL.

III. RESULTS

A. Photoluminescence characterization

The PL acquired from the regions subject to ion implantation was first characterized considering the emission wavelengths >565 nm in order to assess the effects of the ion implantation as a function of the irradiation fluence, including the possible formation of additional types of luminescent defects such as the NV center. Confocal maps of the implanted regions were acquired with a fixed excitation optical power of 0.7 mW, showing arrays of bright spots compatible with the implantation pattern, i.e., located with a regular spacing of 3 μm [Fig. 2(a)]. The points irradiated with a spot dose between 66 and 660 ions/spot were distinguishable from the background, while it was not possible to identify any periodic spot distribution in the areas irradiated at lower fluences. It is worth noticing that also for the 66 and 132 ions/spot dose arrays not all the irradiated spots are emitting photons, a result compatible with the low formation yield of the GeV$^-$ center and the Poisson statistics affecting ion implantation at low absolute numbers of implanted ions.

A randomly chosen subset of the spots fabricated at each fluence was spectrally characterized. All analyzed spots presented the fingerprint of the GeV$^-$ color center emission, namely, a pronounced ZPL (Zero Phonon Line) at 602 nm. Figure 2(b) shows six representative emission spectra acquired at different implantation fluences, together with the background signal acquired in the immediate proximity of the implanted spots. The PL intensity was found to correlate with the implantation fluence, exhibiting a higher contribution from the spots implanted with a higher number of Ge ions.

This finding is also shown from a spatial point of view in Fig. 2(c), where the PL maps corresponding to each implanted region were acquired by restricting the spectral window to the 600–650 nm range to minimize background fluorescence. The analysis was performed on $10 \times 10\,\mu$m^2 PL scan areas to mitigate possible misalignments of the sample surface with respect to the focal plane of the confocal microscope. In order to quantitatively correlate the PL intensity from GeV$^-$ centers to the implantation fluence, 32 emitting spots were selected from each region to take into account the statistical variability introduced by the Poissonian

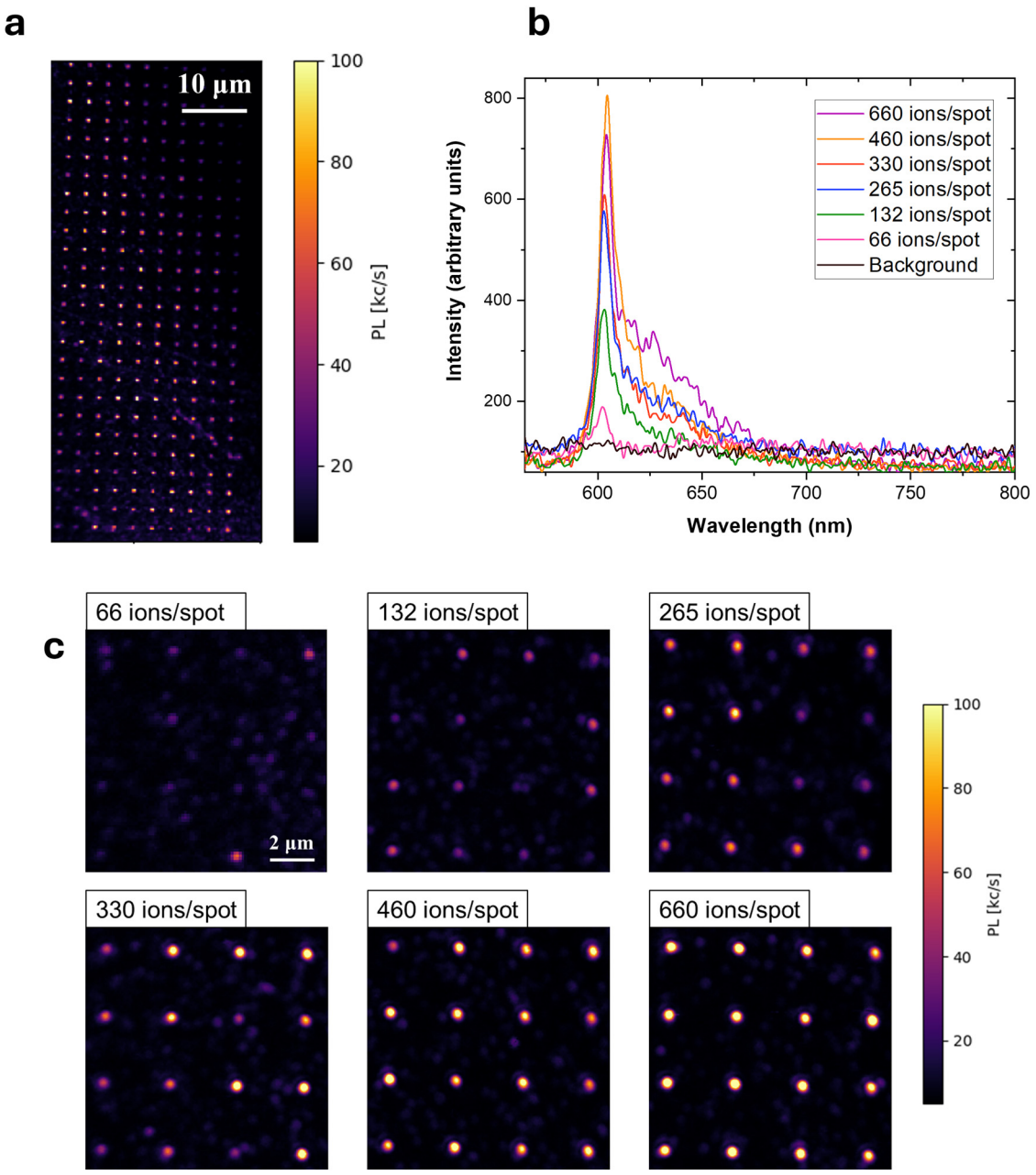

FIG. 2. (a) Confocal PL map of an array implanted with 660 ions/spot. (b) Emission spectra of spots corresponding to visible arrays, acquired using a laser power of 0.7 mW. The spectral resolution is 1 nm. The spectra are not corrected by the background. (c) PL maps of implantation arrays at different ion spot doses, specified by the corresponding label. Acquisition performed in the optical window (600–650) nm, with a laser power of 0.7 mW.

distribution in the number of implanted ions per spot. The PL intensity quantification was conducted by focusing the laser beam at the center of each analyzed spot, using a single measurement, as each spot has a diffraction-limited size.

The integrated PL intensity in the considered spectral range from each emitting spot was corrected by the removal of the background PL associated with residual laser excitation (6 kcps, measured in close proximity to the luminescent spots), which resulted

to be independent from the selected region. The average values, thus, calculated are reported in Table I.

B. Single-photon emitter characterization

Isolated single-photon emitting GeV$^-$ centers were identified consistently in the arrays implanted at the 66 ions/spot dose [Fig. 3(a)]. The occurrence of GeV$^-$ emission at the bright spots regularly spaced according to the implantation grid layout was verified by spectral analysis. The randomly placed emitting spots visible elsewhere in the map are mainly associated with NV emission originating from native defects present in the substrate or a small amount of Ge arriving at the surface as neutrals and, thus, not driven like the ionic species. The GeV$^-$ emission in the 600–650 nm spectral range was characterized by HBT interferometry on a set of 10 randomly selected centers. The results from an exemplary GeV$^-$ emitter are shown in Fig. 3(b). The measurement of the second order autocorrelation function $g^{(2)}(\tau)$ was considered to test the single-photon emitting nature of the candidate diffraction-limited spots. The three-level model was adopted, according to the form $g^{(2)}(\tau) = 1 - (1 + a)\exp(-|\tau| \cdot \lambda_1) + a \cdot \exp(-|\tau| \cdot \lambda_2)$, in order to take into account a moderate bunching effect already reported for the GeV$^-$ center in previous works.[16,21] No background correction was applied to the acquired interferograms, providing a characterization of the single centers as they stand in the specific environment in which they were fabricated. The criterion adopted to verify the occurrence of an individual emitter was the observation of a $g^{(2)}(\tau = 0) < 0.5$ antibunching.[39] For the exemplary case presented in Fig. 3, the resulting $g^{(2)}$ reaches a minimum value of 0.36 for a zero delay time, clearly indicating the occurrence of a single emitting defect. For the specific measurement reported in Fig. 3(b), the total PL intensity recorded was 81 kcps with a background luminescence of 14 kcps, as evaluated by probing the sample in the immediate proximity of the spot under consideration. The nature of the emission was then validated by spectral analysis [Fig. 3(c)], evidencing the 602 nm signature of the GeV$^-$ ZPL.

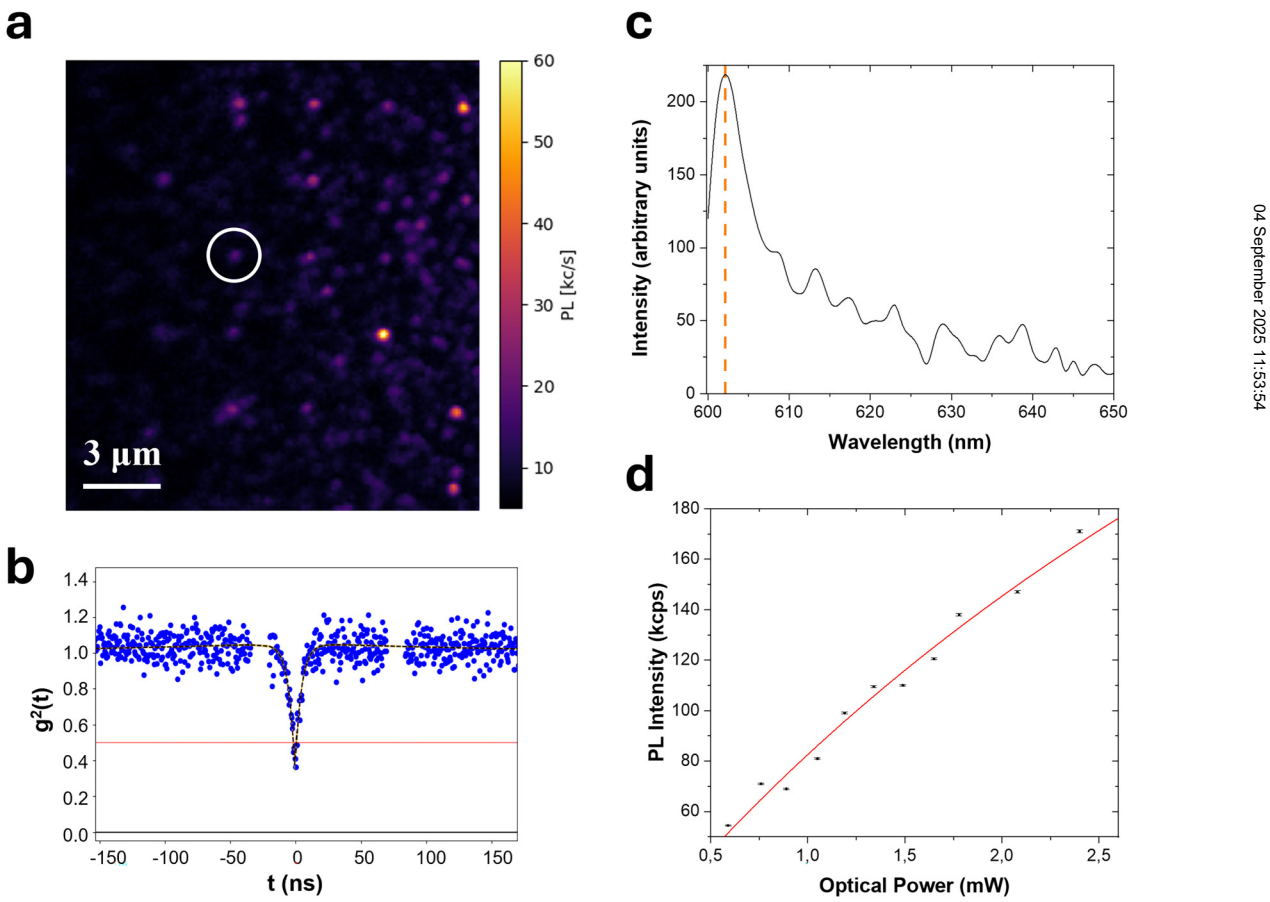

FIG. 3. (a) Confocal PL map of an array implanted with a spot dose of 66 ions/spot. (b) Antibunching profile of the second order autocorrelation function obtained from a HBT interferometric measurement of the spot highlighted in (a), using an optical power of 0.9 mW. The missing data points correspond to the backflash peaks originating from the fiber-coupled HBT interferometer, which were removed for the sake of readability. (c) Emission spectrum of a single GeV$^-$ center; the dashed orange line is at 602 nm wavelength. (d) Saturation curve of the same spot.

TABLE II. Average values of the parameters considered to characterize each single GeV^- center.

Lifetime (ns)	4.5 ± 0.5
PL intensity at saturation (kcps)	440 ± 40
Optical power at saturation (mW)	4.0 ± 0.6

The study of the $g^{(2)}(\tau)$ interferograms was performed at different optical excitation powers in the 0.7–2.0 mW range. The linear dependence of the λ_1 fitting parameter on the excitation power enabled to determine the radiative lifetime of the center.[17] Regarding the single GeV^- center considered in Fig. 3, the calculated radiative lifetime was (4.7 ± 0.3) ns. A table summarizing the average values extracted from the set of 10 GeV^- centers is reported in Table II.

Furthermore, the background-subtracted saturation behavior of each analyzed GeV^- center was studied in the optical power range 0.6–2.4 mW. The collected PL was focused into the core of a fiber-fused 50:50 beam splitter. The PL intensity was measured at both outputs of the beam splitter, acquiring signals corresponding to the emitter under investigation and the background at a distance of a few micrometers, for each fiber branch. This resulted in four total measurements of PL intensity: two for the emitter (S_1 and S_2) and two for its associated background (B_1 and B_2). The uncertainty associated with these measurements was treated assuming the PL count rate as Poisson-distributed. The total PL intensity of the emitter was calculated as $S = (S_1 + S_2 - B_1 - B_2)$, and error propagation was applied accordingly. Each measurement exhibited a stable PL count rate over time, thus ruling out blinking ascribable to further emission from surrounding, optically unstable color centers. The measured data points for the same exemplary center discussed above are shown in Fig. 3(d). The saturation profile was analyzed using the model $I(P) = I_{sat} \cdot P/(P + P_{sat})$,[16,21] resulting in a PL intensity at saturation of $I_{sat} = (580 \pm 60)$ kcps achieved at an optical power $P_{sat} = (5.5 \pm 0.8)$ mW. While these values are higher than the maximum optical power available for the excitation of the emitter, the values extrapolated from the fitting procedure are compatible with what is reported in previous works adopting similar implantation energies and annealing temperatures.[21,22,40]

The average value of the investigated parameters (lifetime, PL emission at saturation, and excitation optical power at saturation) over the set of 10 considered emitters is also reported in Table II. These are in line with the emission properties of the GeV^- center previously reported in the scientific literature.[16,21,22]

C. Formation yield

The quantification of the formation efficiency for the specific fabrication procedure here reported was achieved by considering the integrated background-subtracted PL intensity measured by the single photon avalanche diodes (SPADs) as a function of the implantation ion spot dose reported in Table I and Sec. III A. This value was normalized to the PL count rate of a single GeV^- center as obtained from the characterization performed in Sec. III B. Particularly, the reference single-photon PL intensity, equal to $I_{SPS} = (33 \pm 4)$ kcps, was determined by averaging the count rate

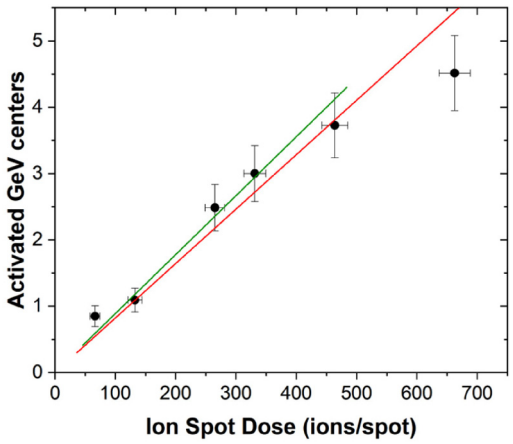

FIG. 4. Optically activated GeV^- color centers as a function of the number of actual implanted Ge++ ions. The red line corresponds to the linear fit considering all the data points, while the green one is related to the linear fit carried out excluding the data point at the highest spot dose.

detected from the set of 10 considered single emitters. The measurement was performed at the same 0.7 mW optical power adopted for the characterization presented in Fig. 2. The ratio between the fluence-dependent PL intensity reported in Table II and I_{SPS} corresponds, thus, to the average number of emitters fabricated at each implanted spot as a function of the Ge^{++} ion spot dose (Fig. 4). Assuming a direct proportionality between the displayed quantities, i.e., neglecting possible saturation effects occurring at high implantation fluences, a linear regression (red line superimposed to the data points in Fig. 4) was performed to evaluate the formation yield η_{eff} of GeV^- centers, according to the equation: $N_{GeV} = \eta_{eff} \cdot N_{ions}$., i.e., imposing the absence of PL emission in the unimplanted substrate. The value obtained for the formation yield can be, thus, estimated as $\eta_{eff} = (0.82 \pm 0.06)$ %.

It is worth observing that the PL intensity corresponding to the highest ion implantation spot dose suggests the occurrence of a saturation behavior, already reported in the scientific literature,[16,41] and related to the accumulation of an amount of implantation-induced lattice damage not recoverable by thermal annealing. This observation is in line with the comparable PL intensity of the GeV^- ZPL observed for the two highest implantation fluences reported in the spectra in Fig. 2(b). If an additional linear fit is performed excluding the highest implantation spot dose (green line in Fig. 4), a formation efficiency of $\eta'_{eff} = (0.89 \pm 0.06)\%$ is found, i.e., a value statistically compatible with the previous estimate. Thus, the value determined by considering the full dataset is sufficient to offer a reliable quantification of the formation yield for the fabrication process under test. This result is in line with the previous reports available in the scientific literature,[34,35] despite the higher implantation fluence adopted, and is smaller with respect to what was found for different diamond color centers (5–10)% fabricated with similar procedures and parameters.[26,42]

The limiting factor in the GeV^- formation yield can be ascribed to the poor structural formation efficiency of the point defect in diamond. This interpretation is justified by the recent

experimental report on the preferential accommodation of implanted Ge ions at substitutional sites[43] rather than at a bond-centered position, the latter being a prerequisite for the split-vacancy optically active configuration. Furthermore, the structural formation yield drops further, below 10%, at an annealing temperature of 900 °C,[43] despite the thermal process is needed both to enhance vacancy migration for the formation of split-vacancy complexes around bond-centered Ge ions and to optically activate the emission of the GeV^- centers. This behavior differs significantly from other split-vacancy centers in diamond which share the same split-vacancy structure, for which the fraction of sites compatible with the split-vacancy configuration can reach 40%.[44–47] Nonetheless, there are additional factors that can hinder the complete formation of split-vacancy defects, which can cause a discrepancy between the probability of the implanted ion stopping in the bond-centered position and the actual formation yield of the color center. The discrepancy can derive from lattice damage and disorder not completely restored or from a not optically active nor stable charge state. These limitations are shared by all the split-vacancy color centers. However, by analogy with some of them, the difference for GeV^- centers is given by the low probability for the Ge ion to occupy the appropriate lattice site to structurally form the color center.

IV. CONCLUSIONS

In this work, the formation yield of the GeV^- color center in diamond upon keV ion implantation and subsequent thermal annealing was quantified. A systematic fabrication process was adopted, exploiting FIB technology to take advantage of nanometric spatial accuracy in the ion delivery and a controllable implantation fluence, which potentially enables an ion spot dose down to single-ion level. The delivery of a low number of ions on a nm-sized specific target was achieved. This fabrication approach favors scalability and is crucial from the perspective of performing deterministic ion implantation. On the other hand, it poses a significant technical challenge, as this may increase lattice disorder due to the accumulation of radiation damage on a nanometric area. The PL analysis of the GeV^- centers, including single emitter characterization, was performed to assess the yield of the GeV^- center formation under the implemented fabrication approach. The obtained formation yield was quantified as (0.82 ± 0.06) %. It has been demonstrated indeed for other types of defects that this limitation can be mitigated by the hot implantation technique,[46] although this approach cannot guarantee the stabilization of the split-vacancy structural configuration of the GeV^- center. Conversely, when compared to other color centers created using similar methodologies, the primary constraint on the GeV^- center formation yield appears to be the favorable lattice configuration as a substitutional site.[43] This observation is in line with the results found in this work and in other previous investigations,[34,35] which suggest that the formation yield is capped below 2% in the case of annealing temperature up to 1200 °C.

Further optimization of the implantation process will be crucial to favor the placement of Ge ions at interstitial sites. The implantation energy does not appear to noticeably influence the formation yield in the 35–200 keV range, as it can be deduced by comparing the results obtained in previous studies[34,35] with our observations. Conversely, an upper limit for the ion fluence should be carefully identified to prevent excessive damage to the diamond lattice. Additionally, the effect of post-implantation processes on the formation yield can be systematically investigated, with a particular emphasis on significantly higher annealing temperature or high-pressure high-temperature (HPHT) treatments, which could offer a tool to promote a more significant rearrangement of the lattice structure.[21]

ACKNOWLEDGMENTS

This work was supported by the following projects: Project "Piemonte Quantum Enabling Technologies" (PiQuET), funded by the Piemonte Region within the "Infra-P" scheme (POR-FESR 2014-2020 program of the European Union); the experiment GeVIon-Q funded by the Q@TN consortium; the experiments ROUGE, QUISS, and PICS4ME funded by the 5th National Commission of the Italian National Institute for Nuclear Physics (INFN); and the "Training on LASer fabrication and ION implantation of DEFects as quantum emitters" (LasIonDef) project, funded by the European Research Council under the "Marie Skłodowska-Curie Innovative Training Networks" program (Grant Agreement No. 956387). We acknowledge financial support under the National Recovery and Resilience Plan (NRRP), Mission 4, Component 2, Investment 1.1, Call for tender No. 1409 published on 14.9.2022 by the Italian Ministry of University and Research (MUR), funded by the European Union—NextGenerationEU—Project No. P2022KSTSR—Opto-mechanical effects in spin-defects for quantum technologies—CUP D53D23019370001. The project contributing to this work 23NRM04 NoQTeS has received funding from the European Partnership on Metrology, co-financed from the European Union's Horizon Europe Research and Innovation Programme and by the Participating States. The work by E.R. and G.G. was supported by the MUR scholarship "PNRR DM 351/2022-M4C1." R.D.A., E.M., and A.B. acknowledge financial support from PNRR MUR Project PE0000023-NQSTI. D.G. and E.S. acknowledge the EU HE project: Experimental production capabilities for quantum technologies in Europe, Qu-Pilot Project No. 101113983.

AUTHOR DECLARATIONS

Conflict of Interest

The authors have no conflicts to disclose.

Author Contributions

Vanna Pugliese: Conceptualization (equal); Data curation (equal); Formal analysis (equal); Investigation (equal); Methodology (equal); Writing – original draft (equal). **Gaia Gavello:** Data curation (equal); Investigation (equal); Methodology (equal); Writing – review & editing (equal). **Elena Nieto Hernandez:** Data curation (equal); Investigation (equal); Writing – review & editing (equal). **Elisa Redolfi:** Data curation (equal); Formal analysis (equal); Investigation (equal); Methodology (equal); Writing – review & editing (equal). **Elia Scattolo:** Investigation (equal); Methodology (equal); Writing – review & editing (equal). **Alessandro Cian:** Investigation (equal); Methodology (equal); Writing – review &

editing (equal). **Elena Missale:** Data curation (equal); Writing – review & editing (equal). **Alberto Bortone:** Investigation (equal); Writing – review & editing (equal). **Rossana Dell'Anna:** Data curation (equal); Funding acquisition (equal); Project administration (equal); Writing – review & editing (equal). **Sviatoslav Ditalia Tchernij:** Conceptualization (equal); Investigation (equal); Project administration (equal); Supervision (equal); Writing – review & editing (equal). **Damiano Giubertoni:** Conceptualization (equal); Funding acquisition (equal); Investigation (equal); Methodology (equal); Project administration (equal); Supervision (equal); Writing – review & editing (equal). **Jacopo Forneris:** Conceptualization (equal); Funding acquisition (equal); Investigation (equal); Project administration (equal); Supervision (equal); Validation (equal); Writing – original draft (equal).

DATA AVAILABILITY

The data that support the findings of this study are available from the corresponding author upon reasonable request.

REFERENCES

[1]J. Wrachtrup and F. Jelezko, "Processing quantum information in diamond," J. Phys.: Condens. Matter **18**(21), S807–S824 (2006).
[2]I. Aharonovich and E. Neu, "Diamond nanophotonics," Adv. Opt. Mater. **2**(10), 911–928 (2014).
[3]C. Bradac, W. Gao, J. Forneris, M. E. Trusheim, and I. Aharonovich, "Quantum nanophotonics with group IV defects in diamond," Nat. Commun. **10**(1), 5625 (2019).
[4]M. Chipaux, K. J. van der Laan, S. R. Hemelaar, M. Hasani, T. Zheng, and R. Schirhagl, "Nanodiamonds and their applications in cells," Small **14**(24), 1704263 (2018).
[5]A. Mzyk, A. Sigaeva, and R. Schirhagl, "Relaxometry with nitrogen vacancy (NV) centers in diamond," Acc. Chem. Res. **55**(24), 3572–3580 (2022).
[6]G. Petrini *et al.*, "Nanodiamond–quantum sensors reveal temperature variation associated to hippocampal neurons firing," Adv. Sci. **9**(28), 2202014 (2022).
[7]I. V. Fedotov *et al.*, "All-optical brain thermometry in freely moving animals," ACS Photonics **7**(12), 3353–3360 (2020).
[8]J. R. Weber *et al.*, "Quantum computing with defects," Proc. Natl. Acad. Sci. U.S.A. **107**(19), 8513–8518 (2010).
[9]S. Pezzagna and J. Meijer, "Quantum computer based on color centers in diamond," Appl. Phys. Rev. **8**(1), 011308 (2021).
[10]G. Bayer *et al.*, "Optical driving, spin initialization and readout of single SiV− centers in a Fabry-Perot resonator," Commun. Phys. **6**(1), 300 (2023).
[11]E. I. Rosenthal *et al.*, "Single-shot readout and weak measurement of a Tin-vacancy qubit in diamond," Phys. Rev. X **14**(4), 041008 (2024).
[12]K. Senkalla, G. Genov, M. H. Metsch, P. Siyushev, and F. Jelezko, "Germanium vacancy in diamond quantum memory exceeding 20 ms," Phys. Rev. Lett. **132**(2), 026901 (2024).
[13]A. Gruber, A. Dräbenstedt, C. Tietz, L. Fleury, J. Wrachtrup, and C. von Borczyskowski, "Scanning confocal optical microscopy and magnetic resonance on single defect centers," Science **276**(5321), 2012–2014 (1997).
[14]M. W. Doherty, N. B. Manson, P. Delaney, F. Jelezko, J. Wrachtrup, and L. C. L. Hollenberg, "The nitrogen-vacancy colour centre in diamond," Phys. Rep. **528**(1), 1–45 (2013).
[15]C. Hepp *et al.*, "Electronic structure of the silicon vacancy color center in diamond," Phys. Rev. Lett. **112**(3), 036405 (2014).
[16]T. Iwasaki *et al.*, "Germanium-vacancy single color centers in diamond," Sci. Rep. **5**(1), 12882 (2015).
[17]S. D. Tchernij *et al.*, "Single-photon-emitting optical centers in diamond fabricated upon Sn implantation," ACS Photonics **4**(10), 2580–2586 (2017).
[18]S. Ditalia Tchernij *et al.*, "Single-photon emitters in lead-implanted single-crystal diamond," ACS Photonics **5**(12), 4864–4871 (2018).
[19]W. B. Gao, A. Imamoglu, H. Bernien, and R. Hanson, "Coherent manipulation, measurement and entanglement of individual solid-state spins using optical fields," Nat. Photonics **9**(6), 363–373 (2015).
[20]B. Machielse *et al.*, "Quantum interference of electromechanically stabilized emitters in nanophotonic devices," Phys. Rev. X **9**(3), 031022 (2019).
[21]E. Nieto Hernández *et al.*, "Efficiency optimization of Ge-V quantum emitters in single-crystal diamond upon ion implantation and HPHT annealing," Adv. Quantum Technol. **6**(8), 2300010 (2023).
[22]J. Christinck *et al.*, "Bright single-photon emission from a GeV center in diamond under a microfabricated solid immersion lens at room temperature," J. Appl. Phys. **133**(19), 193102 (2023).
[23]J.-W. Fan *et al.*, "Germanium-vacancy color center in diamond as a temperature sensor," ACS Photonics **5**(3), 765–770 (2018).
[24]B. Vindolet *et al.*, "Optical properties of SiV and GeV color centers in nanodiamonds under hydrostatic pressures up to 180 GPa," Phys. Rev. B **106**(21), 214109 (2022).
[25]A. Dharmasiri *et al.*, "Sensitivity and heat penalty in all-optical quantum thermometry with germanium-vacancy color centers in diamond," Appl. Phys. Lett. **125**(9), 091102 (2024).
[26]T. Lühmann, J. Meijer, and S. Pezzagna, "Charge-assisted engineering of color centers in diamond," Phys. Status Solidi (a) **218**(5), 2000614 (2021).
[27]Z. Ju, J. Lin, S. Shen, B. Wu, and E. Wu, "Preparations and applications of single color centers in diamond," Adv. Phys.: X **6**(1), 1858721 (2021).
[28]T. Shinada, H. Koyama, C. Hinoshita, K. Imamura, and I. Ohdomari, "Improvement of focused ion-beam optics in single-ion implantation for higher aiming precision of one-by-one doping of impurity atoms into nano-scale semiconductor devices," Jpn. J. Appl. Phys. **41**(Part 2, No. 3A), L287–L290 (2002).
[29]T. Schenkel *et al.*, "Solid state quantum computer development in silicon with single ion implantation," J. Appl. Phys. **94**(11), 7017–7024 (2003).
[30]F. Watt *et al.*, "The National University of Singapore high energy ion nano-probe facility: Performance tests," Nucl. Instrum. Methods Phys. Res. Sect., B **210**, 14–20 (2003).
[31]J. Meijer *et al.*, "Towards the implanting of ions and positioning of nanoparticles with nm spatial resolution," Appl. Phys. A **91**(4), 567–571 (2008).
[32]K. Höflich *et al.*, "Roadmap for focused ion beam technologies," Appl. Phys. Rev. **10**(4), 041311 (2023).
[33]N. Bassim, K. Scott, and L. A. Giannuzzi, "Recent advances in focused ion beam technology and applications," MRS Bull. **39**(4), 317–325 (2014).
[34]Y. Zhou *et al.*, "Direct writing of single germanium vacancy center arrays in diamond," New J. Phys. **20**(12), 125004 (2018).
[35]N. H. Wan *et al.*, "Large-scale integration of artificial atoms in hybrid photonic circuits," Nature **583**(7815), 226–231 (2020).
[36]J. F. Ziegler, M. D. Ziegler, and J. P. Biersack, "SRIM – The stopping and range of ions in matter (2010)," Nucl. Instrum. Methods Phys. Res. Sect., B **268**(11–12), 1818–1823 (2010).
[37]F. Picollo *et al.*, "Effects of high-power laser irradiation on sub-superficial graphitic layers in single-crystal diamond," Acta Mater. **103**, 665–671 (2016).
[38]Y. Bromberg, Y. Lahini, E. Small, and Y. Silberberg, "Hanbury Brown and Twiss interferometry with interacting photons," Nat. Photonics **4**(10), 721–726 (2010).
[39]Grünwald, "Effective second-order correlation function and single-photon detection," New J. Phys. **21**(9), 093003 (2019).
[40]E. Redolfi *et al.*, "Integration of germanium-vacancy single photon emitters arrays in diamond nanopillars," EPJ Quantum Technol. **12**, 25 (2025).
[41]J. E. Fröch *et al.*, "Versatile direct-writing of dopants in a solid state host through recoil implantation," Nat. Commun. **11**(1), 5039 (2020).
[42]T. Lühmann, R. John, R. Wunderlich, J. Meijer, and S. Pezzagna, "Coulomb-driven single defect engineering for scalable qubits and spin sensors in diamond," Nat. Commun. **10**(1), 4956 (2019).
[43]U. Wahl *et al.*, "Structural formation yield of GeV centers from implanted Ge in diamond," Mater. Quantum Technol. **4**(2), 025101 (2024).

[44]E. Corte *et al.*, "Magnesium-vacancy optical centers in diamond," ACS Photonics **10**(1), 101–110 (2023).
[45]U. Wahl *et al.*, "Direct structural identification and quantification of the split-vacancy configuration for implanted Sn in diamond," Phys. Rev. Lett. **125**(4), 045301 (2020).
[46]V. Pugliese *et al.*, "Photoactivation of color centers induced by CW laser irradiation in ion-implanted diamond," ACS Photonics **12**(7), 3803–3814 (2025).
[47]E. Nieto Hernandez *et al.*, "Efficient fabrication of high-density ensembles of color centers via Ion implantation on a hot diamond substrate," Adv. Phys. Res. **3**(12), 2400067 (2024).